

Analysis of multifunctional piezoelectric metastructures for low-frequency bandgap formation and energy harvesting

C Sugino and A Erturk[✉]

G.W. Woodruff School of Mechanical Engineering, Georgia Institute of Technology, Atlanta, GA, United States of America

E-mail: alper.erturk@me.gatech.edu

Received 24 December 2017, revised 21 March 2018

Accepted for publication 26 March 2018

Published 3 May 2018



Abstract

Vibration-based energy harvesting is a growing field for generating low-power electricity to use in wireless electronic devices, such as the sensor networks used in structural health monitoring applications. Locally resonant metastructures, which are structures that comprise locally resonant metamaterial components, enable bandgap formation at wavelengths much longer than the lattice size, for critical applications such as low-frequency vibration attenuation in flexible structures. This work aims to bridge the domains of energy harvesting and locally resonant metamaterials to form multifunctional structures that exhibit both low-power electricity generation and vibration attenuation capabilities. A fully coupled electromechanical modeling framework is developed for two characteristic systems and their modal analysis is presented. Simulations are performed to explore the vibration and electrical power frequency response maps for varying electrical load resistance, and optimal loading conditions are presented. Case studies are presented to understand the interaction of bandgap formation and energy harvesting capabilities of this new class of multifunctional energy-harvesting locally resonant metastructures. It is shown that useful energy can be harvested from locally resonant metastructures without significantly diminishing their dramatic vibration attenuation in the locally resonant bandgap. Thus, integrating energy harvesters into a locally resonant metastructure enables a new potential for multifunctional locally resonant metastructures that can host self-powered sensors.

Keywords: metamaterials, energy harvesting, piezoelectricity, vibration, multifunctional

(Some figures may appear in colour only in the online journal)

Introduction

Vibration-based energy harvesting has received dramatically growing attention over the last two decades [1–7]. The main research motivation for this field derives from the reduced power requirement of small electronic components, such as the wireless sensor networks used in passive and active monitoring applications. The ultimate goal in this research area is to power such small electronic devices by using the vibrational energy available in their environment. In this way, the requirement of an external power source, as well as the maintenance costs and the chemical waste due to conventional

batteries, can be reduced, if not totally eliminated. The three basic vibration-to-electric energy conversion mechanisms are the electromagnetic [8, 9], electrostatic [10, 11] and piezoelectric [12–14] transduction techniques. Other techniques that have received less attention include magnetostriction [15, 16] and the use of electroactive polymers [17, 18]. The main advantages of piezoelectric materials in energy harvesting are their high power density and ease of application. Voltage outputs in electromagnetic energy harvesting are typically very low and often multi-stage post-processing is required to reach a voltage level that can charge a storage component. In piezoelectric energy harvesting, however, usable voltage outputs

can be obtained directly from the piezoelectric material itself. In electrostatic energy harvesting, an input voltage or charge needs to be applied so that the relative vibratory motion of the capacitor elements creates an alternating electrical output. The voltage output in piezoelectric energy harvesting emerges from the constitutive behavior of the material, which eliminates the requirement of an external voltage input. As another advantage, piezoelectric devices can be fabricated in micro-scale owing to the well-established thick-film and thin-film fabrication techniques [3]. Various piezoelectric energy harvester configurations have been developed lately, including both linear and nonlinear piezoelectric energy harvesters, such as linear cantilevers [12–14] as well as bistable beam [4, 19, 20] and bistable plate [4, 21] configurations.

In a separate body of work, researchers have long investigated phononic crystals for their potential to filter or redirect elastic waves [22]. Phononic crystals exhibit bandgaps (i.e. frequency ranges where elastic or acoustic waves cannot propagate) produced by Bragg scattering [23–25], which occurs when the wavelength of the incident wave is on the order of the lattice constant of the crystal [26, 27]. Therefore, a fundamental limitation of Bragg-based phononic crystals is that it is only possible to create low-frequency bandgaps using very large structures. In their seminal work, Liu *et al* [28] showed the potential for locally resonant metamaterials to create bandgaps at wavelengths much larger than the lattice size, enabling the creation of low-frequency bandgaps in relatively small structures. Locally resonant metamaterials contain resonating elements, whether mechanical [28, 29] or electromechanical [30–32], which are capable of storing and transferring energy. A significant body of research has examined locally resonant elastic/acoustic metamaterials of various types. Ho *et al* [29] examined a similar system to the one in Liu *et al* [28] using a rigid frame with rubber-coated metal spheres as resonators. For that type of system, Liu *et al* [33] found analytic expressions for the effective mass densities of 3D and 2D locally resonant metamaterials, showing that the effective mass becomes negative near the resonant frequency. Simplifying the analysis, others used lumped-mass models to obtain the locally resonant bandgap [34, 35]. Other researchers have studied different implementations for resonators for different types of elastic waves [36–42], and two-degree-of-freedom resonators [43]. Moving towards analytical predictions for the bandgap edge frequencies, Xiao *et al* [44] used the plane wave expansion method to study flexural waves in a plate with periodically attached resonators, yielding a method to predict the edges of the bandgap. Peng and Pai [45] also studied a locally resonant metamaterial plate, finding an explicit expression for the bandgap edge frequencies.

In the existing literature, the combination of energy harvesting and vibration attenuation was explored mainly for the classical vibration absorber configuration (e.g. Ali and Adhikari [46]). Beyond the well-known vibration absorbers, locally resonant metastructures are natural choices for the inclusion of vibrational energy harvesters [47], as they already include numerous resonating elements that can be used to harvest energy. This leads to the idea of multifunctional locally resonant metastructures that, in addition to showing

dramatic vibration reduction in a locally resonant bandgap, can recover low-power electricity for sensing or other applications. Recently, we developed modal analysis frameworks for metastructures made from locally resonant metamaterials under bending vibration [48–50]. In the following, we bridge the domains of vibration energy harvesting and locally resonant metamaterials to enable multifunctional energy harvesting-metastructures (based on the Euler–Bernoulli beam theory, i.e. for transverse vibrations/waves). We present an analytical electromechanical framework for two multifunctional energy harvesting locally resonant metastructures, one with mechanical resonators as energy harvesters, and another made from a piezoelectric bimorph with segmented electrodes, shunted with inductors and resistors to add local resonance but also harvest useful energy. For ease of reference, the structure with mechanical resonators as energy harvesters will be referred to as the ‘mechanical metastructure’, while the piezoelectric bimorph with segmented electrodes will be referred to as the ‘electromechanical metastructure’ although clearly both systems are electromechanical in nature.

Mechanical locally resonant metastructure with energy harvesters

Consider a mechanical metastructure whose governing equations are altered from the form presented in [50] to add piezoelectric coupling to the resonator equations:

$$\mathcal{L}[w(\mathbf{P}, t)] + m(\mathbf{P})\ddot{w}(\mathbf{P}, t) - \sum_{j=1}^S (k_j u_j(t) + c_j \dot{u}_j(t))$$

$$\delta(\mathbf{P} - \mathbf{P}_j) = f(\mathbf{P}, t), \quad \mathbf{P} \in D \quad (1)$$

$$m_j \ddot{u}_j + c_j \dot{u}_j + k_j u_j - \vartheta_j v_j = -m_j \ddot{w}(\mathbf{P}_j, t) \quad (2)$$

$$C_{p,j} \dot{v}_j + \mathcal{B}_j[v_j] + \vartheta_j \dot{u}_j = 0 \quad (3)$$

where \mathcal{L} is a linear, self-adjoint differential operator (called the ‘stiffness operator’) of order $2p$, where $p \geq 1$ is an integer defining the order of the system, $w(\mathbf{P}, t)$ is the displacement of a point \mathbf{P} in the domain D at time t , $m(\mathbf{P})$ is the mass distribution at \mathbf{P} , k_j , c_j , m_j , u_j , and \mathbf{P}_j are the stiffness, damping constant, mass, displacement, and position of the j th resonator respectively, S is the total number of resonators, $\delta(\mathbf{P})$ is the Dirac delta function, $f(\mathbf{P}, t)$ is the external forcing, ϑ_j , $C_{p,j}$ and \mathcal{B}_j are the electromechanical coupling, effective piezoelectric capacitance, and admittance operator of the shunt circuit on the j th resonator. The only damping modeled explicitly in these equations is viscous damping from the resonators, with the understanding that modal damping can be introduced in the discretized equations. An example of such a system would be a beam (the primary structure) with multiple cantilever-type [13] energy harvesters with tip masses as the resonators, as shown schematically in figure 1.

Following a procedure similar to [50], we assume a modal analysis type expansion for w in the mode shapes of the structure without resonators (i.e. the ‘plain structure’)

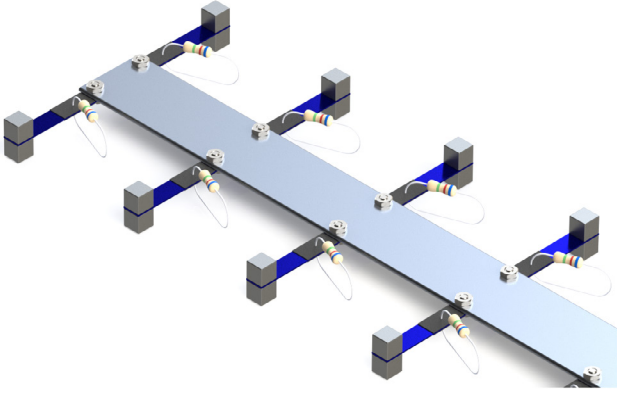


Figure 1. Schematic of the mechanical locally resonant energy harvesting metastructure. Small cantilever beams with tip masses act as mechanical resonators attached to the primary beam structure, and piezoelectric elements with a resistive load are bonded to the mechanical resonators to serve as energy harvesters.

$$w(\mathbf{P}, t) = \sum_{r=1}^N \eta_r(t) \phi_r(\mathbf{P}) \quad (4)$$

where N is the number of modes used in the expansion, $\phi_r(\mathbf{P})$ is the r th mode shape of the plain structure, and $\eta_r(t)$ is the corresponding modal weighting. These mode shapes satisfy the orthogonality conditions

$$\int_D m(\mathbf{P}) \phi_r(\mathbf{P}) \phi_s(\mathbf{P}) dD = \delta_{rs}, \quad r, s = 1, 2, \dots \quad (5)$$

$$\int_D \phi_r(\mathbf{P}) \mathcal{L}[\phi_s(\mathbf{P})] dD = \omega_r^2 \delta_{rs}, \quad r, s = 1, 2, \dots \quad (6)$$

where ω_r^2 is the squared natural frequency of the r th mode shape of the plain structure and δ_{rs} is the Kronecker delta. By substituting equation (4) into equation (1), multiplying by the mode shape ϕ_k , and integrating across the domain, we obtain the discretized version of the primary structure's governing partial differential equation:

$$\ddot{\eta}_r + 2\zeta_r \omega_r \dot{\eta}_r + \omega_r^2 \eta_r - \sum_{j=1}^S (k_j \mu_j + c_j \dot{\mu}_j) \phi_r(\mathbf{P}_j) = q_r, \quad r = 1, 2, \dots, N \quad (7)$$

where

$$q_r(t) = \int_D \phi_r(\mathbf{P}) f(\mathbf{P}, t) dD \quad (8)$$

and ζ_r is the r th modal damping factor. Substituting equation (4) into equations (2) and (3) gives the other two discretized equations:

$$m_j \ddot{\mu}_j + c_j \dot{\mu}_j + k_j \mu_j - \vartheta_j v_j = -m_j \sum_{r=1}^N \phi_r(\mathbf{P}_j) \ddot{\eta}_r \quad (9)$$

$$C_{p,j} \dot{v}_j + \mathcal{Y}_j[v_j] + \vartheta_j \dot{\mu}_j = 0. \quad (10)$$

For a specified set of parameters, equations (7)–(10) can be solved using typical linear multi-degree-of-freedom dynamical systems techniques. Alternatively, taking the Laplace

transforms of equations (7)–(10) and rearranging, the following linear system of equations can be obtained:

$$(s^2 + 2\zeta_r \omega_r s + \omega_r^2) H_r(s) + \frac{s^2 (2\zeta \omega_r s + \omega_r^2) \sum_{j=1}^S m_j \phi_r(\mathbf{P}_j) \sum_{k=1}^N \phi_k(\mathbf{P}_j) H_k(s)}{s^2 + 2\zeta \omega_r s + \omega_r^2 \left(1 + \frac{\gamma s}{s+h(s)}\right)} = Q_r(s) \quad (11)$$

where $H_r(s)$ and $Q_r(s)$ are the Laplace transforms of $\eta_r(t)$ and $q_r(t)$ respectively, $\omega_r^2 = k_j/m_j$ is the short-circuit squared resonant frequency of every resonator, $\zeta = c_j/2\omega_r m_j$ is the damping ratio of every resonator, $h(s) = Y_j(s)/C_{p,j}$ is the normalized shunt circuit admittance of all of the harvesting circuits, where $Y_j(s)$ is the Laplace transform of \mathcal{Y}_j , and γ is a dimensionless coupling term, defined as

$$\gamma = \frac{\vartheta_j^2}{k_j C_{p,j}} \quad (12)$$

which is also assumed to be the same for each resonator. As suggested in [50], the resonator masses m_j can be selected to be proportional to the mass distribution $m(\mathbf{P})$ at the respective resonator locations, or

$$m_j = \mu m(\mathbf{P}_j) \Delta D_j \quad (13)$$

where μ is a dimensionless parameter termed the ‘mass ratio’, defining the ratio of total resonator masses to the mass of the plain structure, and ΔD_j is a portion of the domain D around the j th resonator. With this simplification, we obtain

$$(s^2 + 2\zeta_r \omega_r s + \omega_r^2) H_r(s) + \frac{\mu s^2 (2\zeta \omega_r s + \omega_r^2) \sum_{k=1}^N H_k(s) \sum_{j=1}^S m(\mathbf{P}_j) \phi_r(\mathbf{P}_j) \phi_k(\mathbf{P}_j) \Delta D_j}{s^2 + 2\zeta \omega_r s + \omega_r^2 \left(1 + \frac{\gamma s}{s+h(s)}\right)} = Q_r(s). \quad (14)$$

As the number of resonators becomes sufficiently large, we can use the approximation

$$\sum_{j=1}^S \Delta D_j m(\mathbf{P}_j) \phi_r(\mathbf{P}_j) \phi_k(\mathbf{P}_j) \approx \int_D m(\mathbf{P}) \phi_r(\mathbf{P}) \phi_k(\mathbf{P}) dD = \delta_{rk} \quad (15)$$

such that we obtain

$$\frac{H_r(s)}{Q_r(s)} = \frac{1}{s^2 \left[1 + \frac{\mu (2\zeta \omega_r s + \omega_r^2)}{s^2 + 2\zeta \omega_r s + \omega_r^2 \left(1 + \frac{\gamma s}{s+h(s)}\right)} \right] + 2\zeta_r \omega_r s + \omega_r^2}. \quad (16)$$

When all of the resonators are short-circuited (i.e. $h(s) \rightarrow \infty$) and undamped (i.e. $\zeta = 0$), and for an undamped structure ($\zeta_r = 0$), we obtain the typical locally resonant bandgap as discussed in [50], given by the frequency range

$$\omega_t < \omega < \omega_t \sqrt{1 + \mu}. \quad (17)$$

In the case of open-circuit (i.e. $h(s) = 0$) and undamped resonators, it can be shown that the bandgap appears in the frequency range

$$\omega_t \sqrt{1 + \gamma} < \omega < \omega_t \sqrt{1 + \mu + \gamma}. \quad (18)$$

Thus, the bandgap is shifted to a higher frequency range at open circuit. Generally speaking, since the coupling term γ is

relatively small for real systems, we expect the locally resonant bandgap to be only slightly shifted at open circuit. Depending on the type of shunt circuit used, various types of behavior can be observed. In typical energy harvesting applications, either purely resistive shunts or resistive-inductive shunts are used.

We can obtain the voltage output of the shunt circuit attached to the resonator at location \mathbf{P}_j as

$$V(\mathbf{P}_j, s) = \frac{\vartheta_j}{C_{p,j}} \frac{s}{s + h(s)} \frac{s^2 W(\mathbf{P}, s)}{s^2 + 2\zeta\omega_t s + \omega_t^2 \left(1 + \frac{\gamma s}{s + h(s)}\right)} \quad (19)$$

where $W(\mathbf{P}, s)$ is the Laplace transform of the displacement $w(\mathbf{P}, t)$. The associated complex power can be calculated by substituting $s = i\omega$ for the excitation frequency ω , yielding (after some manipulation)

$$\begin{aligned} \mathbb{S}(\mathbf{P}_j, i\omega) &= |V(\mathbf{P}_j, i\omega)|^2 Y_j^*(i\omega) \quad (20) \\ &= \frac{\mu\gamma\omega^6\omega_t^2 h^*(i\omega) |W(\mathbf{P}_j, i\omega)|^2 m(\mathbf{P}_j) \Delta D_j}{|(i\omega + h(i\omega))(\omega^2 - i2\zeta\omega_t\omega - \omega_t^2) - i\omega\omega_t^2\gamma|^2} \quad (21) \end{aligned}$$

where $()^*$ indicates the complex conjugate. Assuming infinitely many resonators, the total complex power is calculated with the integral

$$\begin{aligned} \mathbb{S}_{tot}(i\omega) &= \sum_{j=1}^S \mathbb{S}(\mathbf{P}_j, i\omega) \approx \int_D d\mathbb{S} \quad (22) \\ &= \frac{\mu\gamma\omega^6\omega_t^2 h^*(i\omega) \int_D m(\mathbf{P}) |W(\mathbf{P}, i\omega)|^2 dD}{|(i\omega + h(i\omega))(\omega^2 - i2\zeta\omega_t\omega - \omega_t^2) - i\omega\omega_t^2\gamma|^2}. \quad (23) \end{aligned}$$

Note that the integral in equation (23) is related to the kinetic energy of the primary beam structure, and an additional factor of ω gives the time rate of change of the kinetic energy. More explicitly,

$$|\dot{T}_{str}(i\omega)| = \frac{1}{2} \omega \int_D m(\mathbf{P}) \omega^2 |W(\mathbf{P}, i\omega)|^2 dD \quad (24)$$

where T_{str} is the kinetic energy of the primary structure. Thus, the total complex power can be written as

$$\mathbb{S}_{tot}(i\omega) = \frac{2\mu\gamma\omega^3\omega_t^2 h^*(i\omega) |\dot{T}_{str}(i\omega)|}{|(i\omega + h(i\omega))(\omega^2 - i2\zeta\omega_t\omega - \omega_t^2) - i\omega\omega_t^2\gamma|^2}. \quad (25)$$

We can also calculate the total complex power easily from the modal weightings $H_r(s)$ by recognizing that the integral in equation (23) can be reduced as

$$\begin{aligned} &\int_D m(\mathbf{P}) |W(\mathbf{P}, i\omega)|^2 dD \\ &= \int_D m(\mathbf{P}) \sum_{r=1}^N H_r(i\omega) \phi_r(\mathbf{P}) \sum_{k=1}^N H_k^*(i\omega) \phi_k(\mathbf{P}) dD = \sum_{r=1}^N |H_r(i\omega)|^2 \quad (26) \end{aligned}$$

where the orthogonality condition of the mode shapes ϕ_r in equation (5) has been used. Thus, the total complex power can also be written as

$$\mathbb{S}_{tot}(i\omega) = \frac{\mu\gamma\omega^6\omega_t^2 h^*(i\omega) \sum_{r=1}^N |H_r(i\omega)|^2}{|(i\omega + h(i\omega))(\omega^2 - i2\zeta\omega_t\omega - \omega_t^2) - i\omega\omega_t^2\gamma|^2}. \quad (27)$$

The simplest type of shunt circuit to quantify energy harvesting performance is a resistor placed across the two electrodes (for AC input - AC output), yielding a normalized admittance $h(i\omega) = 1/\tau$, where $\tau = R_p C_{p,j}$ is the time constant associated with the parallel resistance R_p . To visualize the effect of various load resistances (i.e. values of τ), we consider the structural response and power output for a cantilever beam under base excitation of amplitude w_b at the excitation frequency ω , and plot the tip transmissibility and power output as heatmaps versus τ and ω . Additionally, at each excitation frequency, the optimal value τ_{opt} that maximizes the real part of the power output $P(i\omega) = \text{Re} \{ \mathbb{S}_{tot}(i\omega) \}$ can be obtained, and the resulting optimal real power can be plotted as a function of excitation frequency only. The tip displacement at this optimal loading can also be checked to ensure that the bandgap is still present, even at optimal loading. These plots are shown in figures 2–5 for the mechanical metastructure with energy harvesting resonators.

It is clear from figures 2 and 3 that large, relatively broad-band power output occurs near the resonant frequency of the resonators, just before the locally resonant bandgap. Note that the sudden peaks in both the displacement and power at optimal loading are due to the discrete step size of both frequency and resistance, as the response is extremely sensitive to frequency and resistance in the cluster of modes that appear just before the locally resonant bandgap. In practice, this frequency neighborhood is significantly impacted by both damping and any parameter variations in the system (e.g. slight variations in resonator natural frequency or placement). Large, but narrower-band power output is observed near the resonances of the system. Furthermore, from figures 4 and 5, it is clear that the locally resonant bandgap is largely unchanged by the presence of the harvesting circuitry. The shift from short circuit (small τ) to open circuit (large τ) can be seen as the shift in the frequency range of the locally resonant bandgap. Additionally, the resonant frequencies that appear before the bandgap are strongly attenuated by the harvesting circuit, corresponding to the relatively large power output near the resonant frequency of the resonators. Thus, the use of energy harvesting circuitry integrated with the resonators in a mechanical metastructure can help attenuate the resonances before the locally resonant bandgap while providing useful power for sensing and other applications. Furthermore, the strong attenuation inside the locally resonant bandgap is unchanged, suggesting that such locally resonant metastructures could be designed with integrated energy harvesters to further improve their multifunctionality. The power output from the energy harvesters could be used for low-power sensing, as an example. Additionally, the energy harvesters themselves can act as distributed sensors, as their voltages relate directly to the primary structure's motion.

For relatively small coupling (e.g. figure 5), it is clear that the extreme vibration attenuation properties of the locally resonant bandgap are insensitive to the optimal loading conditions of the energy harvesters. However, it can be expected that for larger coupling γ , the locally resonant bandgap will be more dramatically affected at optimal loading. To study this, the displacement at optimal loading is shown versus

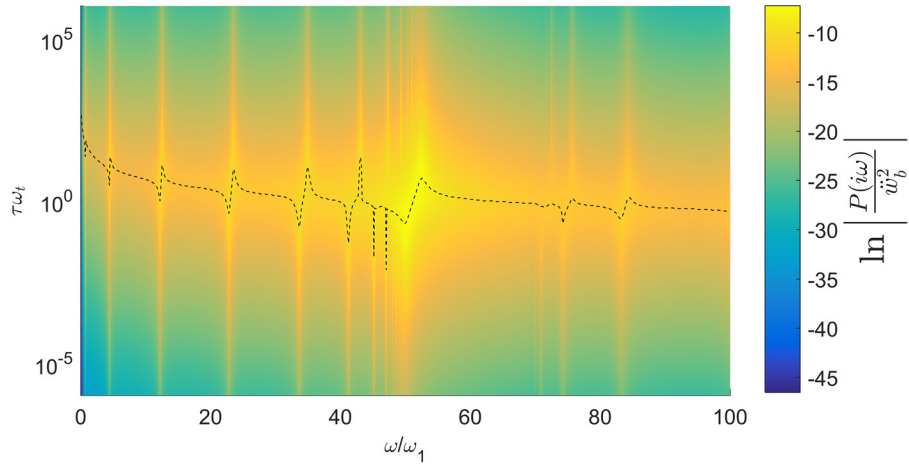


Figure 2. Real power output for the mechanical metastructure versus time constant τ and normalized excitation frequency ω/ω_1 for a cantilever beam excited by base motion, with $\mu = 1$, $\gamma = 0.1$, $\omega_t = 50\omega_1$, $\zeta = 0.01$, $\zeta_r = 0.01$. Dashed line shows the optimal loading at each excitation frequency.

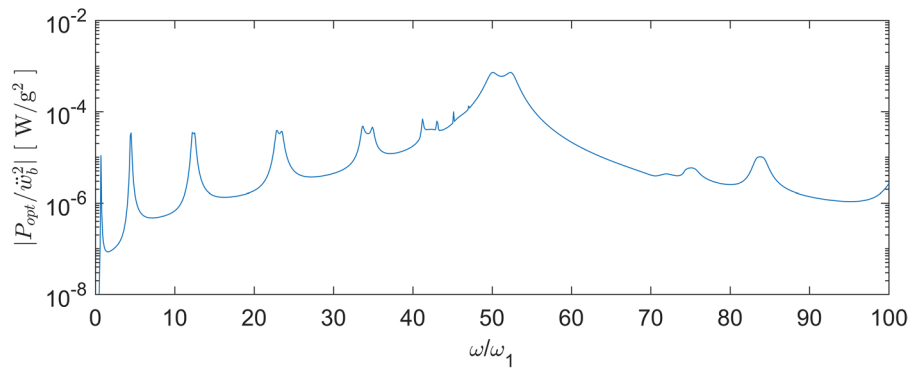


Figure 3. Optimal real power output for the mechanical metastructure with resistive shunting versus normalized excitation frequency ω/ω_1 for a cantilever beam excited by base motion, with $\mu = 1$, $\gamma = 0.1$, $\omega_t = 50\omega_1$, $\zeta = 0.01$, $\zeta_r = 0.01$.

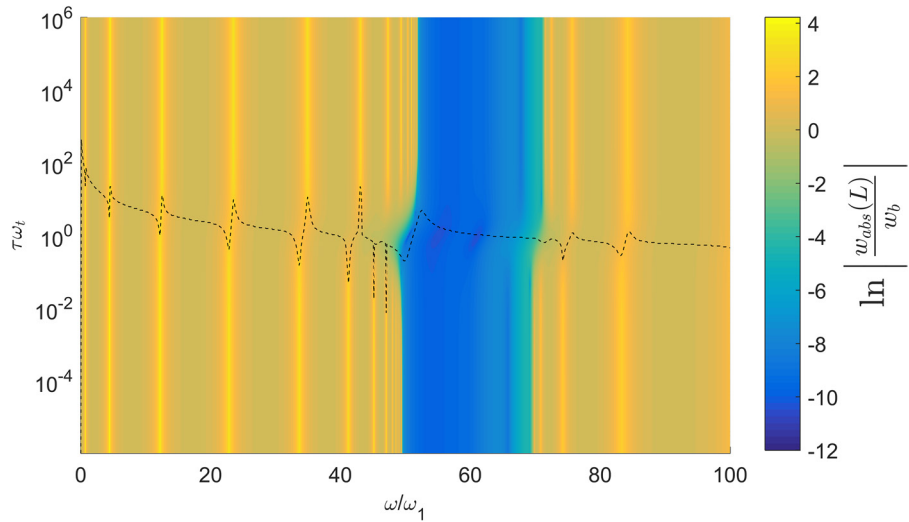


Figure 4. Beam tip response for the mechanical metastructure versus time constant τ and normalized excitation frequency ω/ω_1 for a cantilever beam excited by base motion, with $\mu = 1$, $\gamma = 0.1$, $\omega_t = 50\omega_1$, $\zeta = 0.01$, $\zeta_r = 0.01$. Dashed line shows the optimal loading at each excitation frequency.

excitation frequency ω and electromechanical coupling γ as a heatmap in figure 6. For large electromechanical coupling γ , the displacement at optimal loading bridges between the short and open circuit locally resonant bandgaps, which become more separated for large γ (see equations (17) and (18)). Although the vibration attenuation properties inside the bandgap are slightly reduced, the bandwidth of vibration attenuation is greatly increased. This follows from the

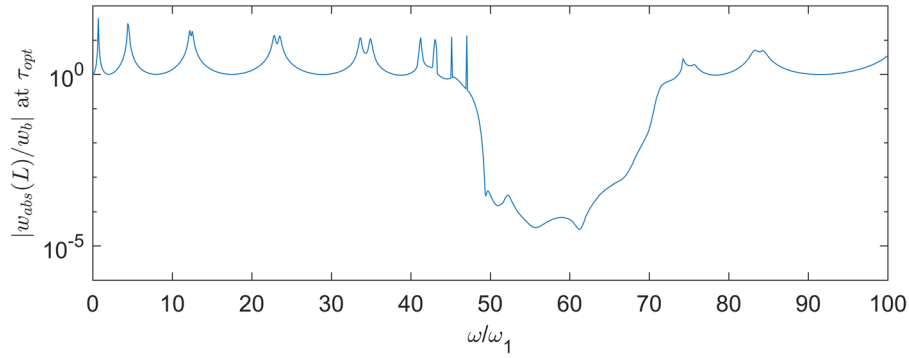


Figure 5. Beam tip response for the mechanical metastructure at optimal power output versus normalized excitation frequency ω/ω_1 for a cantilever beam excited by base motion, with $\mu = 1$, $\gamma = 0.1$, $\omega_t = 50\omega_1$, $\zeta = 0.01$, $\zeta_r = 0.01$.

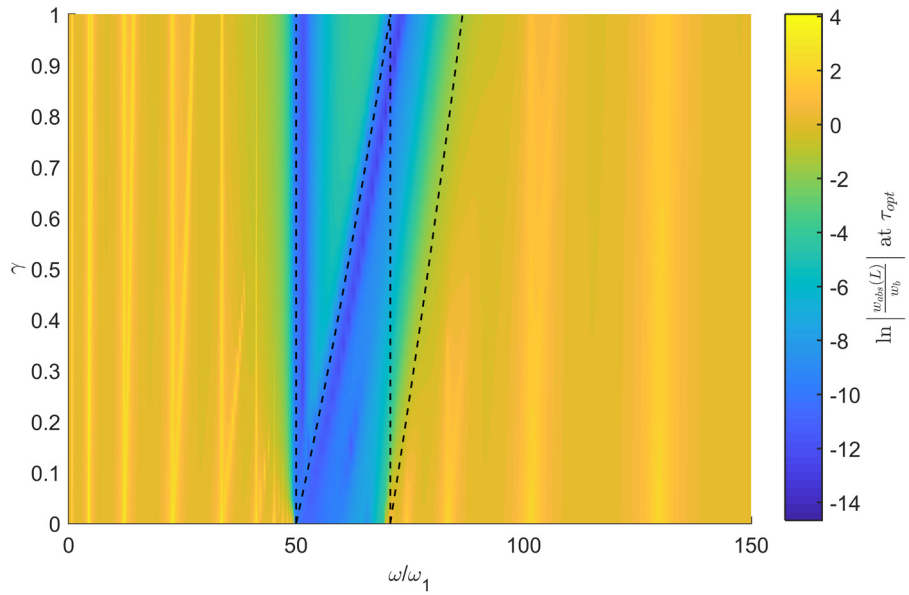


Figure 6. Displacement at optimal loading versus normalized excitation frequency ω/ω_1 and dimensionless coupling γ for $\mu = 1$, $\omega_t = 50\omega_1$, $\zeta = 0.01$, $\zeta_r = 0.01$. The dashed lines show the edge frequencies of the short-circuit and open circuit locally resonant bandgaps (equations (17) and (18)). For large γ values, the optimal resistive loading merges the two distinct bandgaps at open and short circuit.

intuition that higher electromechanical coupling results in higher effective damping at optimal loading, yielding a trade off between bandwidth and amplitude similar to that of a damped vibration absorber. Clearly it would almost always be desirable to have higher electromechanical coupling in the energy harvesters, but this is limited by the piezoelectric materials readily available.

Electromechanical locally resonant metastructure with energy harvesters

Consider a piezoelectric bimorph beam with $j = 1 \dots S$ segmented electrodes placed between left and right positions $x = x_j^L$ and $x = x_j^R$ as considered in [49] with governing equations

$$EI \frac{\partial^4 w}{\partial x^4} + m \frac{\partial^2 w}{\partial t^2} - \vartheta \sum_{j=1}^S v_j(t) \frac{\partial^2}{\partial x^2} [H(x - x_j^L) - H(x - x_j^R)] = f(x, t) \quad (28)$$

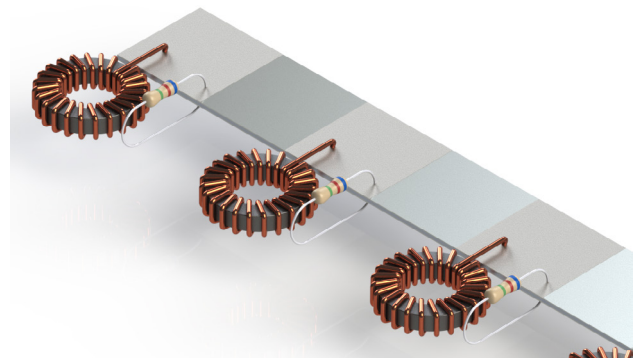


Figure 7. Schematic of the electromechanical locally resonant energy harvesting metastructure. The primary structure is a piezoelectric bimorph with segmented electrodes. Inductors shunted to each pair of electrodes serve as electromechanical resonators, and resistors are placed in parallel to provide energy harvesting capability.

$$C_{p,j} \dot{v}_j(t) + \mathcal{B}_j [v_j(t)] + \vartheta \int_{x_j^L}^{x_j^R} \frac{\partial^3 w}{\partial x^2 \partial t} dx = 0 \quad (29)$$

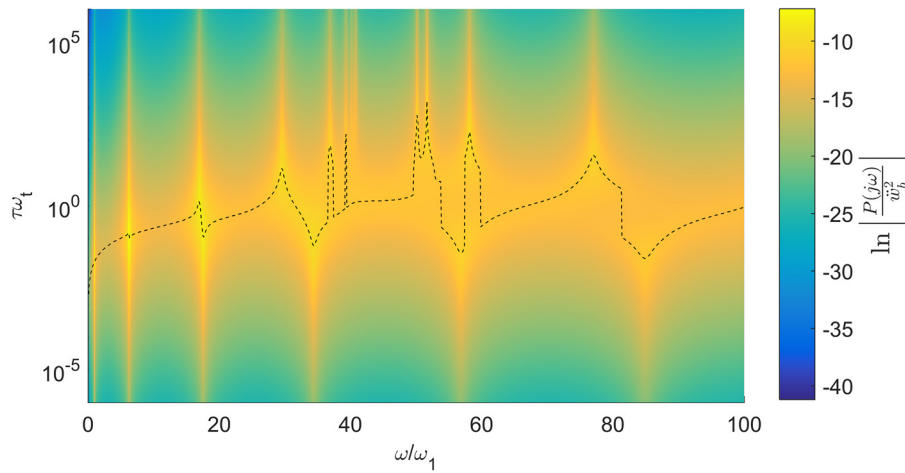


Figure 8. Real power output for the electromechanical metastructure versus time constant τ and normalized excitation frequency ω/ω_1 for a cantilever beam excited by base motion, with $\alpha = 0.44$, $\omega_t = 50\omega_1$, $\zeta_r = 0.01$. Dashed line shows the optimal loading at each excitation frequency.

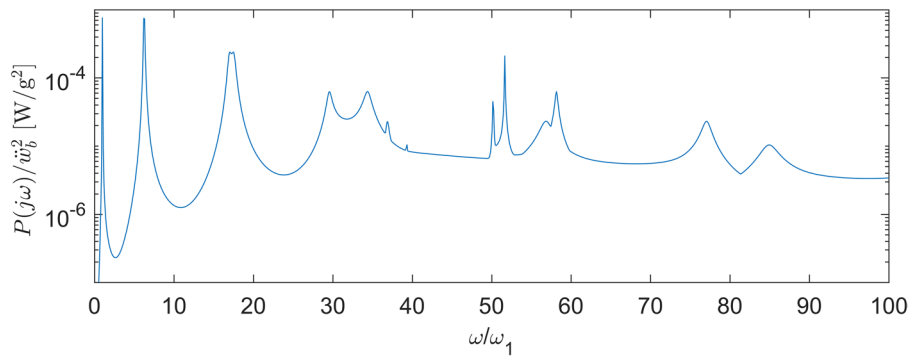


Figure 9. Optimal real power output for the electromechanical metastructure versus normalized excitation frequency ω/ω_1 for a cantilever beam excited by base motion, with $\alpha = 0.44$, $\omega_t = 50\omega_1$, $\zeta_r = 0.01$.

where $w(x, t)$ is the transverse displacement of the beam, $v_j(t)$ is the voltage across the j th pair of electrodes, \mathcal{Y}_j is a linear integro-differential operator corresponding to the admittance of the j th shunt circuit, $H(x)$ is the Heaviside function, and $f(x, t)$ is the external forcing. No damping effects are included, with the understanding that modal damping can be introduced later. The effective properties of the bimorph are

$$EI = \frac{2b}{3} \left(c_s \frac{h_s^3}{8} + \bar{c}_{11}^E \left[\left(h_p + \frac{h_s}{2} \right)^3 - \frac{h_s^3}{8} \right] \right) \quad (30)$$

$$m = b(\rho_s h_s + 2\rho_p h_p) \quad (31)$$

$$\vartheta = \frac{\bar{e}_{31} b_e}{2h_p} \left[\left(h_p + \frac{h_s}{2} \right)^2 - \frac{h_s^2}{4} \right] \quad (32)$$

$$C_{p,j} = \frac{\bar{e}_{33}^S b_e \Delta x_j}{2h_p}. \quad (33)$$

The parameters c_s , ρ_s , and h_s are the central substrate layer’s elastic modulus, mass density, and thickness, respectively, while b is the width of the beam. The piezoelectric layers have mass density ρ_p , thickness h_p , width b , elastic modulus at constant electric field \bar{c}_{11}^E , effective piezoelectric stress constant

\bar{e}_{31} , and permittivity component at constant stress $\bar{\epsilon}_{33}^S$, where the overbars indicate effective properties for 1D thin layers reduced from the full 3D constitutive equations, defined as

$$\bar{c}_{11}^E = \frac{1}{s_{11}^E}, \quad \bar{e}_{31} = \frac{d_{31}}{s_{11}^E}, \quad \bar{\epsilon}_{33}^S = \epsilon_{33}^T - \frac{d_{31}^2}{s_{11}^E} \quad (34)$$

where s_{11}^E is the elastic compliance at constant electric field, d_{31} is the piezoelectric strain constant, and ϵ_{33}^T is the permittivity component at constant strain. Note that the effective piezoelectric capacitance $C_{p,j}$ and admittance \mathcal{Y}_j are now properties associated with the segmented electrodes on the piezoelectric bimorph, rather than properties associated with the individual mechanical resonators as in the previously considered case. Energy harvesting is achieved through the shunts attached to the electrodes on the structure itself, rather than the shunts on the separate mechanical resonators. This system is shown schematically in figure 7.

Because the mathematical development (other than the harvesting part) is similar to [49], only the most relevant results will be reviewed here. By assuming a modal expansion of the same form of equation (4), and using the approximation

$$\sum_{j=1}^S EI \frac{\Delta \phi'_{r,j}}{\Delta x_j} \frac{\Delta \phi'_{k,j}}{\Delta x_j} \Delta x_j \approx \int_0^L EI \frac{d^2 \phi_r}{dx^2} \frac{d^2 \phi_k}{dx^2} dx = \omega_r^2 \delta_{rk} \quad (35)$$

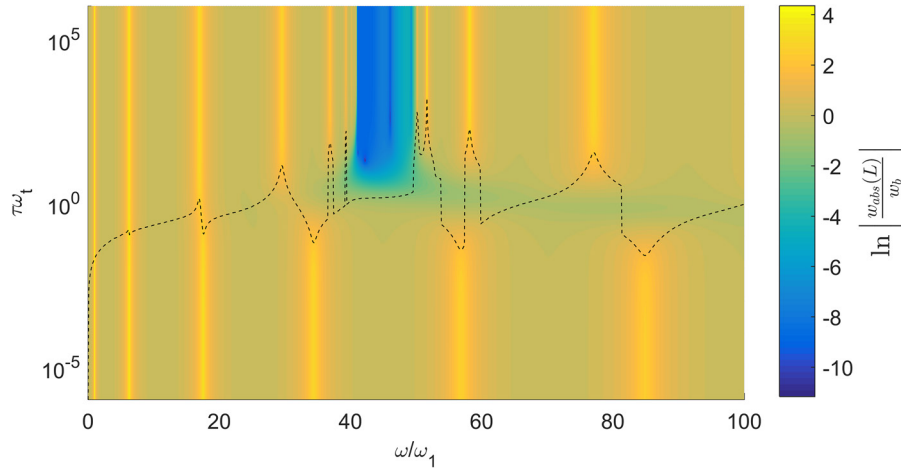


Figure 10. Beam tip response for the electromechanical metastructure versus time constant τ and normalized excitation frequency ω/ω_1 for a cantilever beam excited by base motion, with $\alpha = 0.44$, $\omega_t = 50\omega_1$, $\zeta_r = 0.01$. Dashed line shows the optimal loading at each excitation frequency.

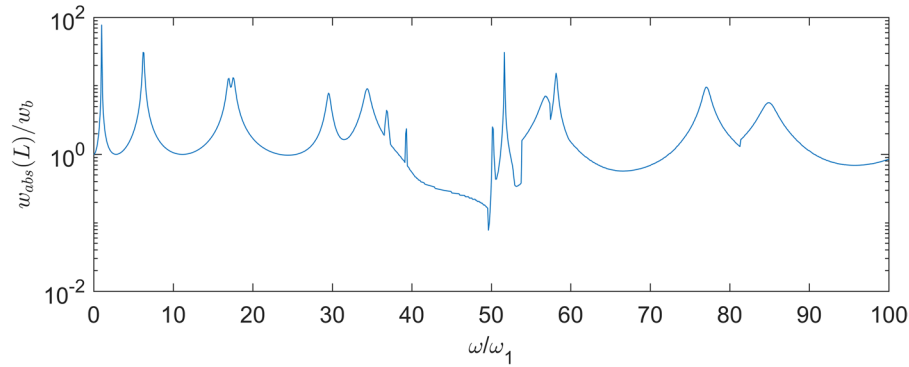


Figure 11. Beam tip response for the electromechanical metastructure at optimal power output versus normalized excitation frequency ω/ω_1 for a cantilever beam excited by base motion, with $\alpha = 0.44$, $\omega_t = 50\omega_1$, $\zeta_r = 0.01$.

where

$$\Delta\phi'_{r,j} = \left(\frac{d\phi_r}{dx}\right)_{x_j^R}^{x_j^L} = \frac{d\phi_r}{dx}(x_j^R) - \frac{d\phi_r}{dx}(x_j^L) \quad (36)$$

it can be shown that the response of the r th mode shape is

$$H_r(s) = \frac{Q_r(s)}{s^2 + 2\zeta_r\omega_r s + \omega_r^2 \left(1 + \frac{\alpha s}{s+h(s)}\right)} \quad (37)$$

where $h(s) = Y_j(s)/C_{p,j}$ is the normalized admittance of the shunt circuits attached to the structure, ζ_r is the r th modal damping factor, and α is a dimensionless electromechanical coupling term, analogous to γ as discussed earlier.

As before, we can obtain the total power through the shunt circuitry by summing the power through each separate shunt circuit, which becomes an integral across the beam in the limit of infinitely many resonators. It can be shown that the total power is then

$$\mathcal{S}_{tot}(i\omega) = \frac{\alpha\omega^2 h^*(i\omega)}{|i\omega + h(i\omega)|^2} \int_0^L EI \left| \frac{d^2}{dx^2} W(x, i\omega) \right|^2 dx \quad (38)$$

where $W(x, i\omega)$ is the beam deflection amplitude at a position x and frequency ω . It is evident that the integral in equation (38) is related to the strain energy, i.e.

$$|\dot{V}_b(i\omega)| = \frac{1}{2}\omega \int_0^L EI \left| \frac{d^2}{dx^2} W(x, i\omega) \right|^2 dx \quad (39)$$

where V_b is the strain energy due to bending in the beam. Thus, the total power produced by the electromechanical structure is

$$\mathcal{S}_{tot}(i\omega) = 2 \frac{\alpha\omega h^*(i\omega)}{|i\omega + h(i\omega)|^2} |\dot{V}_b(i\omega)|. \quad (40)$$

As with the mechanical metastructure, the total power can be calculated easily from the modal weightings by recognizing that

$$\begin{aligned} & \int_0^L EI \left| \frac{d^2}{dx^2} W(x, i\omega) \right|^2 dx \\ &= \int_0^L EI \sum_{r=1}^N H_r(i\omega) \frac{d^2\phi_r}{dx^2} \sum_{k=1}^N H_k^*(i\omega) \frac{d^2\phi_k}{dx^2} dx = \sum_{r=1}^N \omega_r^2 |H_r(i\omega)|^2. \end{aligned} \quad (41)$$

Note that, while the electromechanical metastructure power output is proportional to the electromechanical coupling α , the mechanical metastructure power output is proportional to the added mass ratio μ . The dimensionless coupling α depends on the material properties and geometry of the bimorph and cannot be easily increased, whereas the mass ratio μ can be artificially increased simply by adding mass to

the resonators or reducing the mass of the primary structure, within the design constraints of the system.

Since we consider structures that display both locally resonant behavior and energy harvesting capabilities, a natural choice for the normalized admittance $h(s)$ is that of an inductor placed in parallel with a resistor, or

$$h(s) = \frac{\omega_t^2}{s} + \frac{1}{\tau} \quad (42)$$

where ω_t is the resonant frequency of the shunt circuit, and $\tau = R_p C_{p,j}$ is the time constant associated with the parallel resistance R_p . For $R_p \rightarrow 0$, we would expect to obtain short-circuit behavior, while $R_p \rightarrow \infty$ should yield the typical locally resonant bandgap, which can be shown to exist in the frequency range

$$\frac{\omega_t}{\sqrt{1+\alpha}} < \omega < \omega_t. \quad (43)$$

As with the mechanical locally resonant metastructure, we consider the structural response and power output for a cantilever beam under base excitation of amplitude w_b at the excitation frequency ω , and plot the tip transmissibility and power output as heatmaps versus τ and ω . Additionally, at each excitation frequency, the optimal value τ_{opt} that maximizes the real part of the power output $P(i\omega) = \text{Re} \{S_{tot}(i\omega)\}$ can be obtained, and the resulting optimal real power can be plotted as a function of excitation frequency only. These plots are shown in figures 8–11 for the electromechanical metastructure. For all of the numerical studies shown here, an electromechanical coupling term $\alpha = 0.44$ was used, which is representative of a piezoelectric bimorph made with a single crystal piezoelectric material [49].

As discussed previously, the sudden peaks in optimal power and displacement at optimal loading are due to discretization error near the cluster of modes just before the locally resonant bandgap. As with the mechanical metastructure, it is clear that nontrivial power output can be obtained while maintaining the vibration attenuation properties of the locally resonant bandgap. The optimal power output for the electromechanical metastructure displays more broadband behavior (but less power) than the mechanical metastructure, likely due to the narrow-band nature of mechanical resonator type energy harvesters. Although the maximum power output for the electromechanical metastructure is lower than the mechanical metastructure for these parameter values, the power output is highly sensitive to both the coupling terms γ and α and the added mass ratio μ . Note also that the electromechanical metastructure requires minimal alteration to be adapted for energy harvesting, since the shunt circuitry is already present, whereas the mechanical metastructure needs significant modification. This also means the electromechanical system will be much simpler to adapt to different energy harvesting environments and frequency ranges, with the caveat that extremely low frequencies are difficult to reach due to inductance limitations. Finally, the electromechanical locally resonant metastructure does not require the significant mass addition of the mechanical locally resonant bandgap, although more thorough efficiency analysis is required to

explore how the power output and displacement at optimal loading vary with the total mass of the structure.

Conclusions

The research fields of vibration-based energy harvesting and locally resonant metamaterials have received growing interest lately. The goal in energy harvesting is to generate low-power electricity to use in wireless electronic devices, such as the sensor networks used in structural health monitoring applications. Locally resonant metastructures, which are structures that comprise locally resonant metamaterial components, enable bandgap formation at wavelengths much longer than the lattice size, for critical applications such as low-frequency vibration attenuation in flexible structures. This work couples the domains of energy harvesting and locally resonant metamaterials to form multifunctional structures that exhibit both low-power electricity generation and vibration attenuation capabilities. A fully coupled electromechanical modeling framework is established for two representative multifunctional systems, and their modal analysis is presented. We simulated vibration and electrical power frequency response maps for varying electrical load resistance, demonstrating that even at optimal loading, the locally resonant bandgap can be maintained. The resulting framework can be used to analyze and optimize this new class of multifunctional energy-harvesting locally resonant metastructures. Further challenges lie in designing fully integrated locally resonant metastructures with more complex energy harvesting circuitry with minimal reductions in performance.

Acknowledgments

This work was supported in part by the Air Force Office of Scientific Research grant FA9550-15-1-0397 ‘Integrated multi-field resonant metamaterials for extreme, low frequency damping’.

ORCID iDs

A Erturk  <https://orcid.org/0000-0003-0110-5376>

References

- [1] Anton S R and Sodano H A 2007 A review of power harvesting using piezoelectric materials (2003–2006) *Smart Mater. Struct.* **16** R1–21
- [2] Beeby S P, Tudor M J and White N M 2006 Energy harvesting vibration sources for microsystems applications *Meas. Sci. Technol.* **17** R175–95
- [3] Cook-Chennault K A, Thambi N and Sastry A M 2008 Powering MEMS portable devices—a review of non-regenerative and regenerative power supply systems with special emphasis on piezoelectric energy harvesting systems *Smart Mater. Struct.* **17** 043001
- [4] Erturk A and Inman D J 2011 *Piezoelectric Energy Harvesting* (Chichester: Wiley)

- [5] Elvin N and Erturk A 2013 *Advances in Energy Harvesting Methods* (New York: Springer)
- [6] Roundy S, Wright P K and Rabaey J M 2004 *Energy Scavenging for Wireless Sensor Networks* (Dordrecht: Kluwer)
- [7] Priya S 2007 Advances in energy harvesting using low profile piezoelectric transducers *J. Electroceramics* **19** 167–84
- [8] Glynne-Jones P, Tudor M J, Beeby S P and White N M 2004 An electromagnetic, vibration-powered generator for intelligent sensor systems *Sensors Actuators A* **110** 344–9
- [9] Williams C B, Shearwood C, Harradine M A, Mellor P H, Birch T S and Yates R B 2001 Development of an electromagnetic micro-generator *IEEE Proc. Circuits Devices Syst.* **148** 337–42
- [10] Tvedt L G W, Nguyen D S and Halvorsen E 2010 Nonlinear behavior of an electrostatic energy harvester under wide- and narrowband excitation *J. Microelectromech. Syst.* **19** 305–16
- [11] Mitcheson P D, Miao P, Stark B H, Yeatman E M, Holmes A S and Green T C 2004 MEMS electrostatic micropower generator for low frequency operation *Sensors Actuators A* **115** 523–9
- [12] duToit N E and Wardle B L 2006 Performance of microfabricated piezoelectric vibration energy harvesters *Integr. Ferroelectr.* **83** 13–32
- [13] Erturk A and Inman D J 2009 An experimentally validated bimorph cantilever model for piezoelectric energy harvesting from base excitations *Smart Mater. Struct.* **18** 025009
- [14] Roundy S and Wright P K 2004 A piezoelectric vibration based generator for wireless electronics *Smart Mater. Struct.* **13** 1131–42
- [15] Dai X Z, Wen Y M, Li P, Yang J and Jiang X F 2009 A vibration energy harvester using magnetostrictive/piezoelectric composite transducer *IEEE Sensors* **1** 1374–7
- [16] Hu J, Xu F, Huang A Q and Yuan F G 2011 Optimal design of a vibration-based energy harvester using magnetostrictive material (MsM) *Smart Mater. Struct.* **20** 015021
- [17] Aureli M, Prince C, Porfiri M and Peterson S D 2010 Energy harvesting from base excitation of ionic polymer metal composites in fluid environments *Smart Mater. Struct.* **19** 015003
- [18] Kornbluh R D, Pelrine R, Prahald H, Wong-Foy A, McCoy B, Kim S, Eckerle J and Low T 2011 From boots to buoys: promises and challenges of dielectric elastomer energy harvesting *Electroactive Polym. Actuators Devices* **7976** 797605
- [19] Erturk A, Hoffmann J and Inman D J 2009 A piezomagnetoelastic structure for broadband vibration energy harvesting *Appl. Phys. Lett.* **94** 254102
- [20] Erturk A and Inman D J 2011 Broadband piezoelectric power generation on high-energy orbits of the bistable duffing oscillator with electromechanical coupling *J. Sound Vib.* **330** 2339–53
- [21] Arrieta A F, Hagedorn P, Erturk A and Inman D J 2010 A piezoelectric bistable plate for nonlinear broadband energy harvesting *Appl. Phys. Lett.* **97** 104102
- [22] Laude V 2015 *Phononic Crystals (De Gruyter Studies in Mathematical Physics)* vol 26 (Berlin: de Gruyter & Co)
- [23] Kushwaha M S, Halevi P, Dobrzynski L and Djafari-Rouhani B 1993 Acoustic band structure of periodic elastic composites *Phys. Rev. Lett.* **71** 2022
- [24] Vasseur J, Deymier P A, Chenni B, Djafari-Rouhani B, Dobrzynski L and Prevost D 2001 Experimental and theoretical evidence for the existence of absolute acoustic band gaps in two-dimensional solid phononic crystals *Phys. Rev. Lett.* **86** 3012
- [25] Hussein M I, Hulbert G M and Scott R A 2006 Dispersive elastodynamics of 1D banded materials and structures: analysis *J. Sound Vib.* **289** 779–806
- [26] Hussein M I, Leamy M J and Ruzzene M 2014 Dynamics of phononic materials and structures: historical origins, recent progress, and future outlook *Appl. Mech. Rev.* **66** 040802
- [27] Mace B R 2014 Discussion of ‘Dynamics of phononic materials and structures: historical origins, recent progress and future outlook’ (Hussein M I, Leamy, M J and Ruzzene M 2014 ASME *Appl. Mech. Rev.* **66** 040802) *Appl. Mech. Rev.* **66** 045502
- [28] Liu Z, Zhang X, Mao Y, Zhu Y Y, Yang Z, Chan C T and Sheng P 2000 Locally resonant sonic materials *Science* **289** 1734–6
- [29] Ho K M, Cheng C K, Yang Z, Zhang X X and Sheng P 2003 Broadband locally resonant sonic shields *Appl. Phys. Lett.* **83** 5566–8
- [30] Casadei F, Ruzzene M, Dozio L and Cunefare K A 2010 Broadband vibration control through periodic arrays of resonant shunts: experimental investigation on plates *Smart Mater. Struct.* **19** 015002
- [31] Jin Y, Bonello B and Pan Y 2014 Acoustic metamaterials with piezoelectric resonant structures *J. Phys. D: Appl. Phys.* **47** 245301
- [32] Chen S, Wang G, Wen J and Wen X 2013 Wave propagation and attenuation in plates with periodic arrays of shunted piezo-patches *J. Sound Vib.* **332** 1520–32
- [33] Liu Z, Chan C T and Sheng P 2005 Analytic model of phononic crystals with local resonances *Phys. Rev. B* **71** 014103
- [34] Wang G, Wen X, Wen J, Shao L and Liu Y 2004 Two-dimensional locally resonant phononic crystals with binary structures *Phys. Rev. Lett.* **93** 154302
- [35] Jensen J S 2003 Phononic band gaps and vibrations in one- and two-dimensional mass-spring structures *J. Sound Vib.* **266** 1053–78
- [36] Yang Z, Mei J, Yang M, Chan N and Sheng P 2008 Membrane-type acoustic metamaterial with negative dynamic mass *Phys. Rev. Lett.* **101** 204301
- [37] Oudich M, Senesi M, Assouar M B, Ruzzene M, Sun J-H, Vincent B, Hou Z and Wu T-T 2011 Experimental evidence of locally resonant sonic band gap in two-dimensional phononic stubbed plates *Phys. Rev. B* **84** 165136
- [38] Baravelli E and Ruzzene M 2013 Internally resonating lattices for bandgap generation and low-frequency vibration control *J. Sound Vib.* **332** 6562–79
- [39] Zhu R, Liu X, Hu G, Sun C and Huang G 2014 A chiral elastic metamaterial beam for broadband vibration suppression *J. Sound Vib.* **333** 2759–73
- [40] Matlack K H, Bauhofer A, Krödel S, Palermo A and Daraio C 2016 Composite 3D-printed metastructures for low-frequency and broadband vibration absorption *Proc. Natl Acad. Sci.* **113** 8386–90
- [41] Nouh M, Aldraihem O and Baz A 2015 Wave propagation in metamaterial plates with periodic local resonances *J. Sound Vib.* **341** 53–73
- [42] Wang P, Casadei F, Shan S, Weaver J C and Bertoldi K 2014 Harnessing buckling to design tunable locally resonant acoustic metamaterials *Phys. Rev. Lett.* **113** 014301
- [43] Yu D, Liu Y, Zhao H, Wang G and Qiu J 2006 Flexural vibration band gaps in Euler–Bernoulli beams with locally resonant structures with two degrees of freedom *Phys. Rev. B* **73** 064301
- [44] Xiao Y, Wen J and Wen X 2012 Flexural wave band gaps in locally resonant plates with periodically attached spring-mass resonators *J. Phys. D: Appl. Phys.* **45** 195401

- [45] Peng H and Pai P F 2014 Acoustic metamaterial plates for elastic wave absorption and structural vibration suppression *Int. J. Mech. Sci.* **89** 350–61
- [46] Ali S F and Adhikari S 2013 Energy harvesting dynamic vibration absorbers *J. Appl. Mech.* **80** 041004
- [47] Sugino C, Guillot V and Erturk A 2017 Multifunctional energy harvesting locally resonant metastructures *Conf. on Smart Materials, Adaptive Structures and Intelligent Systems* (American Society of Mechanical Engineers) p V001T07A014
- [48] Sugino C, Leadenham S, Ruzzene M and Erturk A 2016 On the mechanism of bandgap formation in locally resonant finite elastic metamaterials *J. Appl. Phys.* **120** 134501
- [49] Sugino C, Leadenham S, Ruzzene M and Erturk A 2017 An investigation of electroelastic bandgap formation in locally resonant piezoelectric metastructures *Smart Mater. Struct.* **26** 055029
- [50] Sugino C, Xia Y, Leadenham S, Ruzzene M and Erturk A 2017 A general theory for bandgap estimation in locally resonant metastructures *J. Sound Vib.* **406** 104–23